The root-knot nematode effector MiEFF12 targets the host ER quality control system to suppress immune responses and allow parasitism

Salomé Soulé, Kaiwei Huang, Karine Mulet, Joffrey Mejias, Jérémie Bazin, Nhat My Truong, Junior Lusu Kika, Stéphanie Jaubert, Pierre Abad, Jianlong Zhao, et al.

The root-knot nematode effector MiEFF12 targets the host ER quality control system to suppress immune responses and allow parasitism

Salomé Soulé[1, #], Kaiwei Huang[2, #], Karine Mulet[1], Joffrey Mejias[1, 3], Jérémie Bazin[4], Truong Nhat My[1, 5], Junior Lusu Kika[1], Stéphanie Jaubert[1], Pierre Abad[1], Jianlong Zhao[2, *], Bruno Favery[1, *], Michaël Quentin[1, *]

[1] INRAE-Université Côte d'Azur-CNRS, UMR Institut Sophia Agrobiotech, FR-06903 Sophia Antipolis France

[2] State Key Laboratory of Vegetable Biobreeding, Institute of Vegetables and Flowers, Chinese Academy of Agricultural Sciences, 100081, Beijing, China

[3] Present address: CIRAD, UMR PHIM, Montpellier, France

[4] Institute of Plant Sciences Paris-Saclay (IPS2), CNRS, INRAE, Université Paris Saclay - Evry, Université de Paris, Gif sur Yvette 91192, France

[5] Present address: Vietnamese-German Center for Medical Research, 108 Military Central Hospital, Ha Noi, Vietnam

[#] These authors contributed equally to this work.

[*] Authors for correspondence:
Michaël Quentin (michael.quentin@inrae.fr), Bruno Favery (bruno.favery@inrae.fr) and Jianlong Zhao (zhaojianlong@caas.cn).

Summary: 193 words. Text: 6702 words; Figures: 7.
Supplementary informations: 7 supplementary tables and 13 supplementary figures.

Abstract

Root-knot nematodes (RKN) are microscopic parasitic worms able to infest the roots of thousands of plant species, causing massive crop yield losses worldwide. They evade the plant's immune system and manipulate plant cell physiology and metabolism to transform a few root cells into giant cells, which serve as feeding sites for the nematode. RKN parasitism is facilitated by the secretion *in planta* of effector molecules, mostly proteins that hijack host cellular processes. We describe here a conserved RKN-specific effector, EFFECTOR12 (EFF12), which is synthesized exclusively in the esophageal glands of the nematode, and we demonstrate its function in parasitism. In the plant, MiEFF12 localizes to the endoplasmic reticulum (ER). A combination of RNA-sequencing analysis and immunity-suppression bioassays revealed the contribution of MiEFF12 to the modulation of host immunity. Yeast two-hybrid, split luciferase and co-immunoprecipitation approaches identified an essential component of the ER quality control system, the *Solanum lycopersicum* PLANT BAP-LIKE (PBL), and BASIC LEUCINE ZIPPER 60 (BZIP60) proteins as host targets of MiEFF12. Finally, silencing the *PBL* genes in *N. benthamiana* decreased susceptibility to *M. incognita* infection. Our results suggest that EFF12 manipulates PBL function to modify plant immune responses to allow parasitism.

Keywords: *Meloidogyne incognita*, effector, endoplasmic reticulum (ER), ER quality control, *Solanum lycopersicum*, *Nicotiana benthamiana*

1 | INTRODUCTION

Root-knot nematodes (*Meloidogyne spp.*, RKN) are extremely polyphagous plant pathogens responsible for huge losses in agriculture (Jones *et al.*, 2013). These obligate biotrophic root parasites manipulate plant functions to induce a permanent feeding structure. Following root penetration, the RKN second-stage juveniles (J2s) migrate between the cells to reach the vascular cylinder, where they induce the redifferentiation of five to seven selected vascular parenchyma cells into hypertrophied multinucleate feeding cells or "giant cells". These giant cells are the sole source of nutrients for the nematode and are essential for RKN development and reproduction. Concomitantly, the surrounding cells, xylem and phloem proliferate, inducing typical root deformations known as galls or root knots (Favery *et al.*, 2020; Rutter *et al.*, 2022). After successive molts, the adult female RKN lays eggs on the root surface. The success of RKNs as parasites depends on their ability to hijack essential host-cell to induce and maintain a functioning feeding site. The formation of this feeding site is mediated by the secretion into the host of effector proteins essential for RKN parasitism. These effectors hijack host cell processes, including those involved in immune responses, thereby facilitating successful parasitism (Vieira & Gleason, 2019; Rutter et al., 2022).

Plants can detect RKN infestation, which, like infections with other pathogens, triggers immune responses (Kaloshian & Teixeira, 2019; Sato *et al.*, 2019; Siddique *et al.*, 2022). Plants specifically recognize RKN pathogen-associated molecular patterns (PAMPs) or damage-associated molecular patterns (DAMPs) released by the RKN during host invasion, via plasma membrane-associated pattern-recognition receptors (PRRs), which initiate an immune response known as pattern-triggered immunity (PTI) (Sato *et al.*, 2019; Goode & Mitchum, 2022; Siddique *et al.*, 2022; Huang et al. 2023). PTI enables the plant to respond to nematode attack by producing reactive oxygen species (ROS), antimicrobial pathogenesis-related proteins (PR) and metabolites, and by reinforcing their cell walls (Sato *et al.*, 2019; Goode & Mitchum, 2022). In response, pathogens have evolved effector proteins that they secrete into the host to suppress PTI (Jones & Dangl, 2006). Plants have acquired resistance genes enabling them to recognize such effectors specifically, leading to the initiation of effector-triggered immunity (ETI), which results in localized cell death through the hypersensitive response (HR) (Jones & Dangl, 2006;

77 Sato *et al.*, 2019). More than 20 RKN effectors have been reported to be involved in suppression of the
78 PTI or ETI (Rutter *et al.*, 2022). These effectors include MjShKT, which has a *Stichodactyla* toxin
79 (ShKT) domain and is secreted by *Meloidogyne javanica* (Kumar *et al.*, 2023). MjShKT has been
80 implicated in suppression of the ETI and is the only RKN effector known to target the host-plant
81 endoplasmic reticulum (ER) (Kumar *et al.*, 2023).

82 The ER is a highly dynamic organelle consisting of a complex network of cisternae and tubules
83 (Kriechbaumer & Brandizzi, 2020). It is physically connected to the nucleus, the plasma membrane,
84 plastids and mitochondria, and is continuous between cells, via the plasmodesmata (Michaud & Jouhet,
85 2019; Kriechbaumer & Brandizzi, 2020). The ER, thus, participates in intracellular and intercellular
86 communications It is responsible for the biosynthesis and quality control of ER-resident proteins and
87 proteins destined for transportation to the vacuole, plasma membrane or apoplast (Kriechbaumer &
88 Brandizzi, 2020). It is involved in lipid biosynthesis and storage (Kanehara *et al.*, 2022) and is an
89 important organelle for the storage of calcium (Ca^{2+}), an instrumental intracellular messenger (Costa *et*
90 *al.*, 2018) involved in plant immune responses (Köster *et al.*, 2022). The ER can therefore respond and
91 adapt to the biosynthetic requirements imposed on plant cells during plant growth and by environmental
92 stress (Brandizzi, 2021). The ER quality control system (ERQC) identifies misfolded proteins and
93 directs them to the ER-associated degradation (ERAD) machinery (Strasser, 2018). In the absence of
94 such control, the accumulation of unfolded proteins within the ER would trigger ER stress, inducing the
95 unfolded protein response (UPR), leading to the production of proteins of the ERAD pathway and of
96 chaperones responsible for protein refolding, to restore ER homeostasis (Liu & Howell, 2016). If
97 prolonged, the UPR eventually leads to plant cell death (Liu & Howell, 2016).

98 The plant ER and ERQC system components are targeted by several plant pathogen effectors
99 (reviewed by Jing & Wang, 2020; Breeze et al., 2023). For example, proteins acting downstream from
100 ER stress sensors and responsible for inducing the UPR, such as the BZIP60 and NAC transcription
101 factors, have been shown to be targeted by pathogen effectors (Jing & Wang, 2020; Breeze et al., 2023).
102 Similarly, effectors secreted by the oomycete *Phytophthora sojae* interact with ER-resident chaperones,
103 such as plant binding immunoglobulin proteins (BiPs), to suppress host immune responses (Jing *et al.*,

2016). Consistently, plants with an impaired ability to sense ER stress or to trigger the UPR are generally more susceptible to pathogens (Moreno *et al.*, 2012; McLellan *et al.*, 2013; Zhang *et al.*, 2015).

We describe here EFF12, an RKN-specific effector expressed in the dorsal esophageal glands and conserved in different *Meloidogyne* species. We show that MiEFF12 is involved in *M. incognita* parasitism and associates with the host-cell ER. A combination of transcriptomic and molecular analyses indicated that MiEFF12 was involved in suppressing host immune responses. We show that MiEFF12 interacts with the ER-resident PLANT BAP-LIKE (PBL), orthologs of the human B-CELL RECEPTOR-ASSOCIATED PROTEIN 31 (BAP31 or BCAP31) and the BASIC LEUCINE ZIPPER 60 (BZIP60) proteins, two known components of ERQC systems. The silencing of *PBL* genes in *N. benthamiana* decreased susceptibility to *M. incognita*, suggesting a role for this protein in plant defense responses directed against RKN.

2 | RESULTS

2.1 | EFF12 is an RKN-specific effector required for parasitism

MiEFF12s are putative secreted effectors encoded by the M*iEFF12a*/*Minc3s00905g18741/Minc12754* gene and its two paralogs, *MiEFF12b/Minc3s01322g22768/Minc13608* and *MiEFF12c/Minc3s00876g18368/Minc01345* (Abad et al. 2008; Blanc-Mathieu et al., 2017) in *M. incognita*. MiEFF12a, MiEFF12b and MiEFF12c are 96- to 98-amino acid (aa) proteins with a 23- to 25-amino acid signal peptide for secretion (SP) (Figure 1a). Secreted 73-aa MiEFF12 proteins display no similarity to any other sequence in the genus *Meloidogyne* and they carry none of the functional domains listed in public databases. The conserved C-terminal regions are enriched in positively (lysine-K) and negatively (asparagine-D and glutamic acid-E) charged residues. A protein blast search with Wormbase (Kevin et al. 2016) identified one EFF12 homolog in *M. hapla* and four in *M. arenaria* and *M. javanica* (Figure 1b and 1c). A phylogenetic tree constructed from an alignment of 15 EFF12 protein sequences and a pairwise analysis of nucleotide sequence identity revealed variations between copies within the same species and identified MhEFF12 as the most divergent of these effectors (Figure 1b and 1c; Figure S1 and S2). These results indicate that EFF12 is an RKN-specific effector. *MiEFF12* genes

are more strongly expressed at the juvenile parasitic stages than at the J2 pre-parasitic stage, suggesting that EFF12 may play a role in parasitism (Nguyen *et al.*, 2018; Da Rocha *et al.*, 2021).

We analyzed the possible secretion of EFF12 into the plant during parasitism, by using *in situ* hybridization to localize *EFF12* expression in nematode J2s. *MiEFF12* expression was observed exclusively in the dorsal esophageal gland of pre-parasitic *M. incognita* J2s, consistent with previous findings (Nguyen et al., 2018). A similar expression pattern, restricted to the dorsal gland cell, was observed in *M. enterolobii* with an antisense *MeEFF12* probe (Figure 2). Sense probes were used as negative controls and gave no staining in *M. incognita* or *M. enterolobii* (Figure 2).

We investigated the role of MiEFF12 in parasitism through a host-induced gene-silencing approach. We silenced *MiEFF12* during *M. incognita* feeding on *Nicotiana benthamiana,* using the tobacco rattle virus (TRV) for virus-induced gene silencing (VIGS). An empty VIGS construct and a construct targeting the GFP transcript were used as controls. RT-qPCR analyses showed lower levels of *MiEFF12* mRNA in nematodes collected from *N. benthamiana* roots (Figure 3a). Relative to the two controls, the silencing of *MiEFF12* significantly decreased the numbers of both galls and egg masses produced by *M. incognita* on *N. benthamiana* roots six weeks post-infection (Figure 3b). These results demonstrate that MiEFF12 is an effector involved in parasitism.

2.2 | MiEFF12 modulates plant immune responses

Transgenic *Arabidopsis thaliana* lines overexpressing *MiEFF12a* were generated. A large-scale investigation of the possible effects of MiEFF12 secretion on root physiology *in planta* was performed by sequencing the transcripts of wild-type (Col-0) and MiEFF12-expressing *Arabidopsis* (line #C3; Figure S3) roots. The RNA-sequencing data analysis identified 4,080 differentially expressed genes (DEGs) (adjusted *P*-value ≤ 0.01). By analyzing DEGs with a $\log_2$FoldChange of expression ≥ 1 or ≤ -1, we found that 1,103 genes were upregulated and 1,126 were downregulated in the roots of the MiEFF12-expressing line relative to the wild type (Table S1). A gene ontology (GO) enrichment analysis with AgriGO v2.0 showed that genes associated with the GO biological process ‘response to decreased oxygen level’ were overrepresented among the DEGs upregulated in the MiEFF12-expressing line (*P*=4.27e-7; Figure 4a; Table S2 and S3). Thirteen of the 19 genes associated with this GO term are also

upregulated in galls induced by *M. incognita* in *A. thaliana* (Table S3; Yamaguchi et al., 2017). Genes involved in 'defense response' were overrepresented among the 1,126 DEGs downregulated in the MiEFF12a-expressing line (*P*=2.16e-6; Figure 4b; Table S4 and S5). Most of the 103 genes associated with this GO term and downregulated in MiEFF12-expressing *Arabidopsis* encoded nucleotide-binding site (NBS) leucine-rich repeat (LRR) proteins, LRR-receptor kinase like the EF-TU receptor (EFR), receptor-like proteins (RLPs) and PR proteins. These 103 genes included 48 known to be downregulated in galls induced by *M. incognita* (Table S5; Yamaguchi et al., 2017).

Given the role of reactive oxygen species (ROS) in cellular signaling to initiate plant immune responses, we assessed the ability of MiEFF12a to affect the ROS burst induced by the bacterial PAMP flg22 responsible for triggering PTI (Lee *et al.*, 2020). We quantified H_2O_2 in a previously described luminol-based assay (Zhao *et al.*, 2021), in agroinfiltrated *N. benthamiana* leaves with and without *MiEFF12a* expression, after treatment with flg22 or mock treatment. Almost no H_2O_2 production was detected in plant leaves expressing MiEFF12a, whereas an ROS burst was observed in the negative control following treatment with flg22 (Figure 4c). Thus, MiEFF12a abolished the H_2O_2 production associated with PTI.

We also investigated whether MiEFF12a could suppress the programmed cell death physiologically resembling the HR triggered by the mouse pro-apoptotic protein BAX (Lacomme & Santa Cruz, 1999). BAX constructs were introduced into *N. benthamiana* leaves by agroinfiltration 24 h after MiEFF12 or the control construct. As observed for the control, no inhibition of BAX-induced apoptosis was observed when a GFP-MiEFF12a fusion was expressed in the plant (Figure 4d and Figure S3). ETI assays were also performed with the *Globodera pallida* GpRBP-1 protein and the potato Gpa2 resistance protein. GpRBP-1 is recognized by Gpa2 when co-expressed in *N. benthamiana*, triggering an HR (Sacco *et al.*, 2009; Figure 4d). The induction of the Gpa2/GpRBP-1-mediated HR was suppressed by the co-expression of MiEFF12a in *N. benthamiana* leaves (Figure 4e and Figure S3). MiEFF12a suppressed the HR as efficiently as the *Globodera rostochiensis* effector GrCEP12 used as a control (Figure 4e; Chronis et al., 2013). These findings indicate a possible role for MiEFF12 in suppressing plant immunity during plant-nematode interactions.

188 **2.3 | MiEFF12 targets the host-cell endoplasmic reticulum**

189 The subcellular localization of proteins can help to elucidate their function. We localized EFF12 in plant
190 cells by performing transient expression assays in *N. benthamiana* leaves. The coding sequence (CDS)
191 of *MiEFF12a* without the SP was transiently expressed as an N- or C-terminal fusion to GFP under
192 control of the CaMV p35S promoter. The GFP-MiEFF12a fusion was detected in the ER — visualized
193 as a reticulated network at the cell periphery and around the nucleus (Figure 5a). Intriguingly, the signal
194 for the MiEFF12a-GFP fusion was different, displaying localization within large perinuclear structures
195 (Figure 5b). We studied the localization of MiEFF12a further, using an RFP-ER marker (Nelson et al.,
196 2007). With this marker, both the GFP fusions were found to colocalize with the ER marker (Figure 5c
197 and 5d). The use of the RFP-ER marker confirmed that the MiEFF12a-GFP signal associated with
198 perinuclear structures was indeed associated with the ER, the distribution of which was disturbed by the
199 presence of the effector (Figure 5d). These findings indicate that MiEFF12 is an effector targeting the
200 ER, the structure and/or function of which it is capable of altering.
201
202 **2.4 | MiEFF12a interacts with ER-associated proteins**

203 We investigated the function of the MiEFF12 effector in manipulating host cell physiology in more
204 detail by performing a yeast two-hybrid (Y2H) screen to identify direct interactors in tomato. We used
205 MiEFF12a without its signal peptide as a bait, and a tomato root cDNA library from healthy and *M.*
206 *incognita*-infected roots as the prey (Hybrigenics service, France), as previously described (Zhao *et al.*,
207 2020; Mejias *et al.*, 2021). We screened 100 million interactions between MiEFF12 and the cDNA
208 library. We identified two major effector targets, the *Solanum lycopersicum* PLANT BAP-LIKE
209 PROTEINS (SlPBL1 and SlPBL2) and the BASIC REGION/LEUCINE ZIPPER MOTIF 60
210 (SlBZIP60), which were captured 12 and 7 times, respectively (Table S6; Figure S4). Other selected
211 clones carried putative targets captured five times or less (Table S6). Both PBL and BZIP60, known
212 ER-associated proteins involved in ERQC, the ERAD and/or UPR systems (Liu & Howell, 2016;
213 Atabekova *et al.*, 2017), were considered in subsequent analyses.

214 Proteins present in the same subcellular compartment are more likely to be true interactors than those
215 found in different compartments. We therefore performed agroinfiltration experiments to investigate the

subcellular distribution of SlPBL1 and SlBZIP60 in *N. benthamiana* epidermal leaf cells. In *S. lycopersicum*, five genes — *SlPBL1* (*Solyc12g005910*), *SlPBL2* (*Solyc10g053910*), *SlPBL3* (*Solyc09g059570*), *SlPBL4* (*Solyc02g032930*) and *SlPBL5* (*Solyc02g080870*) — encode PBL proteins (Atabekova *et al.*, 2017), whereas SlBZIP60 is encoded by a single gene, *Solyc04g082890* (Kaur & Kaitheri Kandoth, 2021) (Figure S5). The full-length CDS of *SlPBL1* and *SlBZIP60* were cloned to generate fusion proteins with GFP. Coexpression experiments confirmed the colocalization of RFP-MiEFF12 with GFP-SlPBL1 and GFP-BZIP60 in the ER (Figure 6a and 6b). Unlike RFP-MiEFF12 and GFP-SlPBL1, GFP-SlBZIP60 was also observed in the nucleoplasm (Figure 6b). For the SlPBL1-GFP fusion, fluorescence was observed in large perinuclear structures similar to those observed for the MiEFF12a-GFP fusion, while SlBZIP60-GFP was mostly detected in the nucleoplasm (Figure S6). These results confirm that SlPBL and SlBZIP60 are located in the ER and could interact with MiEFF12 *in planta*.

Co-immunoprecipitation assays (Co-IP) were then performed to validate these interactions. The full-length SlPBL1 and its soluble fragment and the full length of SlBZIP60 were fused separately with GFP to generate the SlPBLtotal-GFP, SlPBLsoluble-GFP and GFP-SlBZIP60 constructs, respectively (Figure 6c). These constructs were co-expressed together with MiEFF12a carrying an HA tag (MiEFF12a–HA), in *N. benthamiana* leaves. The complete SlPBL1 and SlBZIP60 proteins were co-immunoprecipitated with MiEFF12a (Figure 6d). Furthermore, because RKN calreticulin (CRT) effectors also localize in the ER when expressed in plant cells (Jaouannet *et al.*, 2013; Liu *et al.*, 2024), we used the *M. incognita* MiCRT1 effector as a negative control. MiCRT1 was unable to interact with the full-length SlPBL1 or with its cytosolic fragment, nor with SlBZIP60 (Fig. 6d). These findings demonstrate that MiEFF12a interacts with SlPBL1 and SlBZIP60 at the ER of the plant cell.

2.5 | *PBLs* promote root-knot nematode parasitism

We then investigated the possible role of PBL and BZIP60 proteins in the plant immune response and RKN parasitism. A knockout *bzip60* Arabidopsis mutant line was challenged with *M. incognita*. Six weeks after inoculation, we observed no significant effect of the *BZIP60* mutation on the number of females producing egg masses (Figure S7a). Similarly, silencing the unique *NbBZIP60* gene in *N.*

benthamiana (*Niben101Scf24096g00018*) through a VIGS approach did not affect RKN development or reproduction (Figure S8 and S7b). These results indicate that plant BZIP60 is not required for RKN parasitism. We then silenced *PBL* genes in *N. benthamiana,* using the TRV for VIGS. Using the SGN VIGS tool (Fernandez-Pozo *et al.*, 2015), we selected six genes encoding NbPBLs in *N. benthamiana*: *NbPBL1a* (*Niben101Scf02543g02013*), *NbPBL1b* (*Niben101Scf08039g00007*), *NbPBL2a* (*Niben101Scf00435g05003*), *NbPBL2b* (*Niben101Scf04477g03012*), *NbPBL3a* (*Niben101Scf02516g00006*) and *NbPBL3b* (*Niben101Scf02145g09007*) (Figure S9). Using a Co-IP approach, we could verify that MiEFF12a could indeed interact with NbPBL1a, NbPBL2a and NbPBL3a (Figure S10). We then designed a chimeric TVR2 construct to silence all *NbPBL* genes. This construct specifically targeted a 200-nucleotide region of each *NbPBL1a/b*, *NbPBL2a/b* and *NbPBL3a/b* pair (Figure S11). A TRV2 targeting a GFP transcript was used as a negative control. The TRV1 and TRV2 were introduced into three-week-old *N. benthamiana* plants with *A. tumefaciens*. Seven days after inoculation (dai), root samples were harvested for RNA extraction, and the remaining plants were inoculated with 200 *M. incognita* J2s (Figure 7a). RT-qPCR was performed to confirm that the targeted *NbPBL* genes in the treated *N. benthamiana* plants were effectively silenced relative to the control (Figure 7b). The plants were recovered six weeks post-infection with *M. incognita.* The plants displayed no macroscopic developmental phenotype, and root weight was not altered by the silencing of *NbPBL* genes (Figure S12). Roots were stained with eosin, and galls and egg masses were counted. In three independent experiments, the numbers of galls and egg masses were found to be significantly smaller in plants with silenced *PBL* genes than in controls (Figure 7c). To uncover PBLs involvement in regulating plant response to RKN infection, we analyzed SlPBL1 function in suppressing plant defenses as described earlier. SlPBL1 could suppress ROS burst triggered by fgl22 in *N. benthamiana* (Figure S13). These results suggest that RKNs hijack the function of the plant PBL proteins, negative regulators of plant defense, to promote host susceptibility to *M. incognita*.

3 | DISCUSSION

3.1 | MiEFF12 is an effector targeting the host ER and involved in defense suppression

Numerous RKN effectors have been reported to suppress plant immunity (Vieira and Gleason; Rutter et al., 2022). MiCRT, a calreticulin secreted into the host apoplast, was the first RKN effector shown to suppress PTI-triggered callose deposition and the induction of PR genes (Jaouannet *et al.*, 2013). Several PTI-suppressing effectors have since been reported, including *M. incognita* MiMIF-2, MiCTL1 and MiPDCD6, and *M. graminicola* MgMO289 (Zhao *et al.*, 2020; Song *et al.*, 2021; Zhao *et al.*, 2021; Kamaruzzaman *et al.*, 2022). RKN effectors have also been implicated in the suppression of ETI-type cell death. The effectors involved include *M. enterolobii* MeTCTP, *M. javanica* Mj10A08 and Mimsp40, which suppress the programmed cell death triggered by the pro-apoptotic Bcl-2 family protein BAX (Hu et al., 2022; Niu et al., 2016; Zhuo et al., 2017). The co-expression of a resistance gene with the corresponding avirulence effector is often used to trigger an HR in such bioassays (Naalden et al., 2018; Nguyen et al., 2018). Low levels of cell death via the HR are triggered by the recognition of *G. pallida* RBP1 proteins by the potato Gpa2 (Carpentier et al., 2013), which can be suppressed by some RKN effectors, such as *M. graminicola* MgMO289 (Song et al., 2021).

We describe here a conserved RKN effector, EFF12, which is produced in the dorsal gland. Despite the absence of a known functional domain, MiEFF12 suppresses the ROS burst induced by the flg22 peptide and the HR triggered by co-expression of the GpRBP1 effector and the potato Gpa2 resistance protein. However, like the HR-suppressing MiSGCR1 effector (Nguyen et al., 2018), MiEFF12 was unable to suppress the strong cell death response induced by BAX. A genome-scaled transcriptomic analysis on an MiEFF12a-overexpressing *Arabidopsis* line further confirmed the function of EFF12 in repressing defense-associated genes.

Transient expression experiments in *N. benthamiana* epidermal leaf cells demonstrated that MiEFF12, while its not having an ER-retention signal, targets the ER. Several RKN effectors, such as MiASP2 and 6D4 (Vieira et al., 2011), have been reported to target the host apoplast, whereas others, such as MiPDI1 and MiCTL-1 are secreted into the cytoplasm (Zhao et al., 2020 and 2021), or target the nucleus, as reported for MiEFF1 and MiEFF18 (Truong et al., 2021; Mejias et al., 2021). Only a few have been reported to target the plant endomembrane system. Several pathogens are known to target the ER to ensure the successful infestation of plants (Jing & Wang, 2020) and MiEFF12 is the third RKN effector demonstrated to target this endomembrane compartment. Kumar *et al.* (2023) recently described

the *M. javanica* MjShKT effector, which localizes to the ER and Golgi compartments when transiently expressed in *N. benthamiana* epidermal leaf cells. However, the host cell targets of MjShKT and the mechanism of its suppression of plant cell death have not yet been identified. MgCRT1 is another RKN effector, secreted into giant cells, that localize in the ER during parasitism (Liu et al., 2024). MgCRT1 was shown to interact with an ER-localised rice calmodulin-like protein OsCML31 to regulate rice immunity and promote susceptibility to *M. graminicola.*

3.2 | PBL is a new host-cell player in RKN parasitism

We identified BZIP60 and PBLs, which are known to be resident in the ER, as the host-cell targets of MiEFF12, consistent with the subcellular distribution reported here for this effector. The full length BZIP60 is anchored in the ER membrane, where its function remains unknown. But when ER stress is elevated, the stress sensor and activator INOSITOL-REQUIRING ENZYME 1 (IRE1) is splicing BZIP60 mRNA, resulting in the production of a transcription factor that can be translocated in the nucleus allowing the UPR to restore ER homeostasis. Roles for IRE1 and BZIP60 in plant immunity have been documented (Bao & Howell, 2017; Jing & Wang, 2020). Our results indicate that suppressing BZIP60 function does not alter plants susceptibility to RKN. The role of other UPR branches, having overlapping functions with IRE1/BZIP60 pathway, in this biotrophic interaction remains, however, to be investigated. B-CELL RECEPTOR-ASSOCIATED PROTEIN 31 (BAP31) is a conserved integral ER-associated protein with three transmembrane domains in its N-terminal region and a C-terminal cytosolic tail (Quistgaard, 2021). In animals, BAP31 has been described as an important chaperone or quality control factor involved in ER membrane protein sorting, promoting protein retention in the ER, transport from the ER to the downstream secretory pathway or other cellular compartments, or targeting to the ERAD system for degradation (Quistgaard, 2021; Wakana et al., 2008). It is also cleaved by caspase and plays a role in apoptosis (Breckenridge et al., 2003; Quistgaard, 2021). The equivalent proteins to BAP31 in plants are probably BAP-like proteins (PBLs) and are encoded by multigene families (Atabekova et al., 2017). The functions of PBLs remain largely undescribed. A PBL from *N. tabacum*, NtPBL, was shown to interact with the tobacco protein Nt-4/1, a protein known to interact with plant virus movement proteins and to affect the long-distance transport of potato spindle tuber

viroid (PSTVd) via the phloem (Pankratenko et al., 2017). Interestingly, NtPBL was shown to induce the relocalization of Nt-4/1 to ER bodies and large aggregates with a granular structure (Pankratenko et al., 2017) similar to those we observed when overexpressing MiEFF12a- or SlPBL1-GFP fusions. In animal cells, the re-localization of BAP31 under stress conditions to a juxta-nuclear ER compartment involved in the ER-associated degradation of misfolded proteins is well documented (Quistgaard, 2021). In addition, the cytosolic tail of NtPBL has been shown to bind RNA (pre-miRNA and viroid RNA), and the expression of *NtPBL* in *N. benthamiana* via a TRV-based approach strongly affects plant development and/or the symptoms induced by TRV (Atabekova et al., 2017). We show here that NbPBLs play a role in RKN parasitism, as plants in which *NbPBL* genes were silenced were less susceptible to *M. incognita*. Furthermore, our finding indicates that PBLs negatively regulate host immunity.

3.3 | MiEFF12 targets plant PBLs to suppress ER-mediated immunity

The ER plays an important role in plant immunity. PRRs are synthesized in the ER and are subject to ER quality control to ensure that they are transported in the correctly folded form from the ER to the plasma membrane (Park & Seo, 2015). As an example, actors of the ER quality control were shown to be involved in the EF-Tu receptor (EFR) biogenesis (Li et al., 2009; Nekrasov et al., 2009). Similarly, antimicrobial PR proteins secreted following recognition of the infesting pathogens are produced and folded at the ER and then processed by the Golgi apparatus for delivery to the apoplast. As a result, the ER is frequently targeted by pathogens and several ER-associated proteins have been implicated in plant responses to pathogen infections (Jing & Wang, 2020). Given the role of BAP31 as a chaperone controlling the fate of the protein — retention in the ER, export, degradation by the ERAD or escape from degradation (Quistgaard, 2021) — we suggest that these functions are conserved in the PBLs of plants and are hijacked by MiEFF12 to prevent the initiation or full expression of PTI. We have shown that MiEFF12a can suppress HR-cell death, possibly through its interaction with SlPBLs. In plants, the ER, or more specifically ER stress, is a recognized initiator of programmed cell death (Eichmann & Schäfer, 2012; Simoni *et al.*, 2022). The role of PBLs in modulating these pathways remains to be elucidated, but the induction of plant cell death programs must be prevented if biotrophic interactions

are to be initiated and maintained throughout the nematode life cycle. Several molecules have already been identified as involved in both PTI and ETI, and PBLs may play such a role at the interaction of the PTI and ETI signaling pathways.

Further analysis would be required to define more precisely the functions of PBLs in regulating plant immunity and the ways in which the effector affects them. This study has taken the first step in this process by revealing a new pathogenic strategy used by RKN to hijack plant metabolism. In this strategy, the MiEFF12 effector targets PBL corrupting their functions so as to promote RKN parasitism. PBL-encoding genes, thus, emerge as promising susceptibility genes that could be targeted in innovative breeding strategies with the aim of generating RKN-resistant crops.

4 | EXPERIMENTAL PROCEDURES

4.1 | Nematode and plant materials

Meloidogyne incognita strain "Morelos" was multiplied in tomato (*S. lycopersicum* cv. "Saint Pierre") grown in a growth chamber (25°C, with a 16 h photoperiod). Freshly hatched J2s were collected as described by Caillaud & Favery (2020). The previously described *bzip60* mutant (SALK_050203; Lu & Christopher, 2008) was obtained from the Arabidopsis Biological Resource Center (ABRC, Ohio State University, Columbus, OH, USA). For VIGS experiments, *N. benthamiana* seeds were sown on soil and incubated at 4°C for two days. After germination, plantlets were transplanted into pots containing soil and sand (1:1) and were grown at 24°C (photoperiod, 16 h light: 8 h dark). For transcriptome analysis, *Arabidopsis* seeds were surface-sterilized and added to liquid MS medium (0.5 x MS salts, 1% sucrose, pH 6.4). They were incubated at 25°C, under a 12-hour period, with gentle shaking (70 rpm), as previously described (Mejias *et al.*, 2021).

4.2 | EFF12 sequence analysis, alignment, and phylogenetic tree

The sequences of putative EFF12 paralogs and orthologs were obtained from *Meloidogyne* genomic resources (http://www6.inra.fr/meloidogyne_incognita and Wormbase parasite). We used 15 *Meloidogyne* EFF12 sequences from *M. arenaria, M. enterolobii, M. incognita, M. floridensis*, and *M.*

384 *javanica* in this analysis. The sequences of the proteins encoded by these genes were analyzed with
385 PHOBIUS and Prosite to identify the SP and to search for putative functional domains, respectively
386 (http://phobius.sbc.su.se/; https://prosite.expasy.org/). EFF12 sequences were aligned with the ClustalW
387 algorithm (Thompson *et al.*, 2003) and their evolutionary history was inferred by maximum likelihood
388 methods, as previously described (Berger *et al.*, 2020). *Meloidogyne hapla* was used as the outgroup for
389 the phylogenetic tree based on putative orthologs of EFF12.

390

391 **4.3 | *In situ* hybridization (ISH)**

392 ISH was performed on freshly hatched *M. incognita* and *M. enterolobii* J2s, as previously described
393 (Jaouannet *et al.*, 2018). For probe production, the MiEFF12a, and MeEFF12 sequences were amplified
394 specifically from entry vectors with the primers MiEFF12_GW3 and MiEFF12_GW5 (for MiEFF12a)
395 or MeEFF12_GW3 and MeEFF12_GW5 (for MeEFF12) (Table S7). Sense probes for MiEFF12a and
396 MeEFF12 were used as negative controls. Photomicrographs were obtained with a Zeiss Axioplan2
397 microscope (Zeiss, Germany).

398

399 **4.4 | RKN infection assay, juveniles in the plant**

400 Three-week-old *Arabidopsis* seedlings were inoculated with 200 *M. incognita* J2s per plant. Roots were
401 collected six weeks after infection and stained with 0.5% eosin. The number of females forming egg
402 masses was then determined. *N. benthamiana* plants subjected to HIGS/VIGS were inoculated with 200
403 *M. incognita* J2s per plant, seven dpi with TRV, and incubated at 24°C. Infected *N. benthamiana* roots
404 were collected six weeks after infection. Galls or egg masses were counted under a binocular
405 microscope, and the root system was weighted.

406

407 **4.5 | Subcellular distribution in the plant**

408 The *M. incognita* MiEFF12 CDS lacking the signal peptide, the *S. lycopersicum* PBL (total and soluble
409 portion) and BZIP60 (unspliced form) were amplified by PCR with specific primers (Table S7) and
410 inserted into the pDON207 donor vector. They were recombined in pK2GW7 (P35S:MiEFF12),

pK7WGR2 (P35S:mRFP-MiEFF12a), pK7FGW2 (P35S:eGFP-SlPBL, P35S:eGFP-SlBZIP60 and P35S:eGFP-MiEFF12a), or pK7FWG2 (P35S:SlPBL-eGFP, P35S:SlBZIP60-eGFP and P35S: MiEFF12a-eGFP) (Karimi *et al.*, 2002) with Gateway technology (Invitrogen). All the constructs were sequenced (GATC Biotech) and transferred into *A. tumefaciens* strain GV3101. Leaves from three- to four-week-old *N. benthamiana* plants were subjected to agroinfiltration with recombinant strains of *A. tumefaciens* containing GFP or RFP vectors, as described by Mejias *et al.* (2021). Leaves were imaged 48 hours after agroinfiltration, with an inverted confocal microscope (LSM 880; Zeiss) equipped with an argon ion laser as the excitation source. Samples were excited at 488 nm for GFP and 543 nm for RFP. GFP and RFP emissions were detected selectively with 505–530 nm and 560–615 nm band-pass emission filters, respectively.

4.6 | Yeast two-hybrid screen

For the Y2H screen, the CDS of the MiEFF12 without the SP was used as a bait. The MiEFF12a sequence was amplified (Table S2) and inserted into the pB27 vector (Hybrigenics Services, Paris, France). The Y2H screen was performed with an infested tomato root cDNA library (Hybrigenics Services, Paris, France), as previously described (Mejias *et al.*, 2021).

4.7 | Host-induced silencing of the MiEFF12a gene and virus-induced silencing of PBL and BZIP60 genes

VIGS/HIGS assays were performed on *N. benthamiana*. For HIGS experiments, fragments of *MiEFF12a* (291 bp) and *GFP* (298 bp) were amplified by PCR with the primers listed in Table S7 and inserted into the TRV2 vector. HIGS experiments were performed as described by Zhao *et al.* (2021), and RT-qPCR were performed to validate the silencing of the MiEFF12 genes 10 dai with the TRV. We used the VIGS-Tool (https://vigs.solgenomics.net/) to design the best sequence for silencing *BZIP60* and *PBL* genes in *N. benthamiana* (Figure S7 and S9). A 300 nucleotides fragment of *NbBZIP60* was PCR-amplified using specific primers (Table S7) before ligation into the TVR2 plasmid. The nucleotide sequences for the following pairs of genes — *NbPBL1a*/*NbPBL1b*, *NbPBL2a*/*NbPBL2b*, *NbPBL3a*/*NbPBL3b* — were sufficiently similar for the design of a chimeric construct targeting 200

nucleotides for each pair synthesized with pUC57 (Gene Universal Inc, Newark DE, USA). The insert was then inserted into the TRV2 plasmid (Figure S9) and the resulting construct was used to transform *A. tumefaciens* strain GV3101. VIGS experiments were performed as previously described (Mejias et al., 2022). Each treatment involved at least 20 *N. benthamiana* plants, and the entire experiment was performed at least twice.

4.8 | Cell death and PTI suppression assay in *N. benthamiana*

The CDS of MiEFF12 and GFP were amplified and inserted into the super1300 vector. The resulting constructs were then used to transform *A. tumefaciens* GV3101. *Agrobacterium* cells carrying BAX or GpRBP1/Gpa2 were used to trigger cell death in *N. benthamiana* leaves (Sacco *et al.*, 2009; Jing *et al.*, 2016). GrCEP12 was used as a positive control to suppress GpRBP1/Gpa2-induced cell death (Chronis et al., 2013). Agro-infiltrations into four-week-old *N. benthamiana* leaves were performed as described elsewhere (Nguyen *et al.*, 2018). Photographs were taken 5 dpi for the assessment of cell death.

For the ROS assays the CDS of MiEFF12 without its native SP and SlPBL1 were inserted into the super 1300 vector. Four-weeks old *N. benthamiana* leaves were infiltrated with *A. tumefaciens* carrying the plasmid, and buffer was used for control. Two days after infiltration, leaf discs were collected and prepared for the ROS assay (luminol-based method) as previously described (Chen *et al.*, 2013).

4.9 | Quantitative RT-PCR

Total RNA was extracted with the RNeasy® Mini kit (Qiagen), and cDNA was synthesized with the SuperScript III First Strand Synthesis system (Invitrogen, Thermo Fisher Scientific, Waltham, MA, USA) according to the manufacturer's instructions. At least three separate biological replicates were performed for each experiment. PCR was performed with Maxima SYBR Green qPCR Master Mix (29; Fermentas, Thermo Fisher Scientific, Waltham, MA, USA) on an I-Cycler (Bio-Rad, CA, USA) with gene-specific primers (Table S1). Quantifications and statistical analyses were performed with SATqPCR (Rancurel *et al.*, 2019).

4.10 | Co-immunoprecipitation assays

For the Co-IP assay, the CDS of MiCRT and MiEFF12a (without the signal peptide sequence) or SlPBL1total, SlPBL1soluble, NbPBL1a, NbPBL2a and NbPBL3a were inserted into the super1300 vectors with a HA-tag and a GFP-tag, respectively, fused to the C-terminal end of the sequence, and SlBZIP60 was cloned into pBIN vector with a GFP-tag fused to the N-terminal of the sequence. Total protein was extracted from four-week-old *N. benthamiana* leaves co-expressing SlPBL1 or SlBZIP60 and MiEFF12a or MiCRT, after 48 h of infiltration. Co-IPs were performed with BeyoMag^{TM} anti-HA Magnetic Beads (Beyotime, China), and the eluted proteins were identified by western blotting with anti-GFP (Beyotime, China) and anti-HA (Beyotime, China) antibodies as described by Zhao *et al.* (2023).

4.11 | Transcriptome analysis

For RNA-seq experiments, seeds were surface-sterilized and sown in liquid MS medium (½MS salts, 1% sucrose, pH 6.4) with gentle shaking (70 rpm), under a 12 h : 12 h, light : dark photoperiod, at 25°C. Roots were collected after 11 days and immediately frozen in liquid nitrogen. Total RNA was extracted with TriZol (Invitrogen), according to the Invitrogen protocol. The RNA was treated with DNAse (Ambion), and its quality and integrity were assessed with a Bioanalyzer (Agilent). Library construction, paired-end sequencing and data analysis were performed as described by Mejias et al. (2021). Gene ontology enrichment analysis was performed with the agriGO v2.0 toolkit (http://systemsbiology.cau.edu.cn/agriGOv2/; Tian *et al.*, 2017), using default parameters.

4.12 | Statistical analysis

Graphs and plots were created with R and Microsoft® Office Excel® 2019. Statistical analyses were performed with R software (R Development Core Team, version 4.1.0). and SATqPCR (https://satqpcr.sophia.inrae.fr/cgi/home.cgi) (Rancurel *et al.*, 2019).

4.13 | Accession numbers

Sequence data from this article can be found in Solgenomics (https://solgenomics.net/) and GenBank/EMBL databases under the following accession numbers: *Meloidogyne incognita*

MiEFF12a/Minc12754 (KX907763), MiCRT/Minc06693 (AF402771.1); *Arabidopsis thaliana* AtBZIP60 (AT1G42990); *Nicotiana benthamiana* NbBZIP60 (Niben101Scf24096g00018), NbPBL1a (Niben101Scf02543g02013), NbPBL1b (Niben101Scf08039g00007), NbPBL2a (Niben101Scf00435g05003), NbPBL2b (Niben101Scf04477g03012), NbPBL3a (Niben101Scf02516g00006), NbPBL3b (Niben101Scf02145g09007); *Solanum lycopersicum* SlBZIP60 (Solyc04g082890), SlPBL1 (Solyc12g005910), SlPBL2 (Solyc10g053910), SlPBL3 (Solyc09g059570), SlPBL4 (Solyc02g032930), SlPBL5 (Solyc02g080870). The transcriptome data are available from the Sequence Read Archive (SRA) under accession number PRJNA641665 and PRJNA719908 (*A. thaliana* Col-0 and P35S:MiEFF12 roots, respectively).

ACKNOWLEDGMENTS

We thank Dr Johnathan Dalzell and Steven Dyer (Queen's University Belfast, UK) for the tomato VIGS protocol and vectors, Prof. S.P. Dinesh-Kumar (University of California, Davis, USA) for VIGS vectors and Hybrigenics Services (Paris, France) for providing the pB27 vector and the L40ΔGal4 yeast strains. We thank Pauline Foubert for taking care of the plant material. Microscopy work was performed at the SPIBOC imaging facility of Institut Sophia Agrobiotech and we thank Dr Olivier Pierre for his help with microscopy. This work was funded by INRAE, by the French Government (National Research Agency, ANR) through the LabEx Signalife (#ANR-11-LABX-0028-01), IDEX UCAJedi (#ANR-15-IDEX-0001), the LabEx Saclay Plant Sciences (#ANR-10-LABX-40) and the MASH project (#ANR-21-CE20-0002), the INRAE-Syngenta Nem-Targetom project, and the National Key Research and Development Program of China (2023YFD1400400). S.S. holds a doctoral fellowship from INRAE SPE department and Université Côte d'Azur. J.M. holds a doctoral fellowship from the French *Ministère de l'Enseignement Supérieur, de la Recherche et de l'Innovation* (MENRT grant). N.M.T. was supported by a USTH fellowship, as part of the 911-USTH program of the Ministry of Education and Training of The Socialist Republic of Vietnam.

AUTHOR CONTRIBUTIONS

S.S., J.Z., B.F. and M.Q. designed the experiments. S.S., K.H., K.M., J.M., J.B, T.N.M., J.L.K. and M.Q. performed the experiments. S.S., J.B., S.J., P.A., J.Z., B.F. and M.Q. analyzed the data. S.J., P.A., J.Z., B.F. and M.Q. obtained funding, and supervised experiments and data analysis. SS., P.A., B.F. and M.Q. wrote the manuscript. All the authors read and edited the final manuscript.

CONFLICT OF INTEREST STATEMENT

The authors have no conflict of interest to declare.

DATA AVAILABILITY STATEMENT

The data supporting the findings of this study are available from the corresponding author upon reasonable request.

REFERENCES

Abad, P., Gouzy, J., Aury, J.M., Castagnone-Sereno, P., Danchin, E.G., Deleury, E. et al. (2008) Genome sequence of the metazoan plant-parasitic nematode Meloidogyne incognita. Nature Biotechnology, 26, 909-15.

Atabekova, A.K., Pankratenko, A.V., Makarova, S.S., Lazareva, E.A., Owens, R.A., Solovyev, A.G. et al. (2017) Phylogenetic and functional analyses of a plant protein related to human B-cell receptor-associated proteins. Biochimie, 132, 28-37.

Berger, A., Boscari, A., Horta Arau´ jo, N., Maucourt, M., Hanchi, M., Bernillon, S. et al. (2020) Plant nitrate reductases regulate nitric oxide production and nitrogen-fixing metabolism during the Medicago truncatula–Sinorhizobium meliloti symbiosis. Frontiers in Plant Science, 11, 1313.

Blanc-Mathieu, R., Perfus-Barbeoch, L., Aury, J.-M.M., Da Rocha, M., Gouzy, J., Sallet, E., et al. (2017) Hybridization and polyploidy enable genomic plasticity without sex in the most devastating plant-parasitic nematodes. PLoS Genetics, 13, e1006777.

von Bargen, S., Salchert, K., Paape, M., Piechulla, B. & Kellmann, J.W. (2001) Interactions between the tomato spotted wilt virus movement protein and plant proteins showing homologies to myosin, kinesin and DnaJ-like chaperones. Plant Physiology and Biochemistry, 39, 1083-1093.

550 Brandizzi F. (2021) Maintaining the structural and functional homeostasis of the plant endoplasmic
551 reticulum. Developmental Cell, 56, 919-932.
552 Breckenridge, D.G., Stojanovic, M., Marcellus, R.C. & Shore, G.C. (2003) Caspase cleavage product
553 of BAP31 induces mitochondrial fission through endoplasmic reticulum calcium signals, enhancing
554 cytochrome c release to the cytosol. Journal of Cell Biology, 160, 1115-1127.
555 Breeze, E., Vale, V., McLellan, H., Pecrix, Y., Godiard, L., Grant, M. et al. (2023) A tell tail sign: a
556 conserved C-terminal tail-anchor domain targets a subset of pathogen effectors to the plant
557 endoplasmic reticulum. Journal of Experimental Botany, 74, 3188-3202.
558 Caillaud, M.C. & Favery, B. (2016) In vivo imaging of microtubule organization in dividing giant cell.
559 Methods in Molecular Biology, 1370,137-44.
560 Carpentier, J., Grenier, E., Esquibet, M., Hamel, L.P., Moffett, P., Manzanares-Dauleux, M.J. et al.
561 (2013) Evolution and variability of Solanum RanGAP2, a cofactor in the incompatible interaction
562 between the resistance protein GPA2 and the Globodera pallida effector Gp-RBP-1. BMC
563 Evolutionary Biology, 13, 87.
564 Chen, H., Zou, Y., Shang, Y., Lin, H., Wang, Y., Cai, R. et al. (2008) Firefly luciferase complementation
565 imaging assay for protein-protein interactions in plants. Plant Physiology 146: 368–376.
566 Chronis, D., Chen, S., Lu, S., Hewezi, T., Carpenter, S.C.D., Loria, R. et al. (2013), A ubiquitin carboxyl
567 extension protein secreted from a plant-parasitic nematode *Globodera rostochiensis* is cleaved in
568 planta to promote plant parasitism. Plant Journal, 74, 185-196.
569 Costa, A., Navazio, L. & Szabo, I. (2018) The contribution of organelles to plant intracellular calcium
570 signalling. Journal of Experimental Botany, 69, 4175-4193.
571 Eichmann, R. & Schäfer, P. (2012) The endoplasmic reticulum in plant immunity and cell death.
572 Frontiers in Plant Science, 3, 1-6.
573 Favery, B., Dubreuil, G., Chen, M.S., Giron, D. & Abad, P. (2020) Gall-inducing parasites: convergent
574 and conserved strategies of plant manipulation by insects and nematodes. Annual Review of
575 Phytopathology, 58, 1-22.

576 Fernandez-Pozo, N., Rosli, H.G., Martin, G.B. & Mueller, L.A. (2015) The SGN VIGS tool: user-
577 friendly software to design virus-induced gene silencing (VIGS) constructs for functional genomics.
578 Molecular Plant, 8, 486-8.
579 Goode, K. & Mitchum, M.G. (2022) Pattern-triggered immunity against root-knot nematode infection:
580 a minireview. Physiologia Plantarum, 174, e13680.
581 Gu, Y., Zavaliev, R. & Dong, X. (2017) Membrane Trafficking in Plant Immunity. Molecular Plant, 10,
582 1026–1034.
583 Hu, L., Lin, B., Chen, J., Song, H., Zhuo, K., & Liao, J. (2022). The effector MJ-10A08 of Meloidogyne
584 javanica is required for parasitism that suppressed programmed cell death in Nicotiana benthamiana.
585 Nematology, 24, 939-952.
586 Huang, L., Yuan, Y., Lewis, C., Kud, J., Kuhl, J.C., Caplan, A., et al. (2023) NILR1 perceives a
587 nematode ascaroside triggering immune signaling and resistance. Current Biology, 33, 3992-3997.
588 Jaouannet, M., Magliano, M., Arguel, M.J., Gourgues, M., Evangelisti, E., Abad, P. et al. (2013) The
589 root-knot nematode calreticulin Mi-CRT is a key effector in plant defense suppression. Molecular
590 Plant-Microbe Interactions, 26, 97-105.
591 Jaouannet, M., Nguyen C.N., Quentin, M., Jaubert-Possamai, S., Rosso, M.N. & Favery, B. (2018) In
592 situ hybridization (ISH) in preparasitic and parasitic stages of the plant-parasitic nematode
593 Meloidogyne spp. Bio-Protocol, 8, 1-13.
594 Jing, M., Guo, B., Li, H., Yang, B., Wang, H., Kong, G. et al. (2016) A Phytophthora sojae effector
595 suppresses endoplasmic reticulum stress-mediated immunity by stabilizing plant Binding
596 immunoglobulin Proteins. Nature Communications, 7, 11685.
597 Jing, M. & Wang, Y. (2020) Plant pathogens utilize effectors to hijack the host endoplasmic reticulum
598 as part of their infection strategy. Engineering, 6, 500-504.
599 Jones, J.D.G. & Dangl, J.L. (2006) The plant immune system. Nature, 444, 323-329.
600 Jones, J.T., Haegeman, A., Danchin, E.G.J., Gaur, H.S., Helder, J., Jones, M.G.K. et al. (2013) Top 10
601 plant-parasitic nematodes. Molecular Plant Pathology, 14, 946-961.
602 Kaloshian, I. & Teixeira, M. (2019) Advances in plant-nematode interactions with emphasis on the
603 notorious nematode genus Meloidogyne. Phytopathology, 109, 1988-1996.

Kamaruzzaman, M., Zhao, L-F., Zhang, J-A., Zhu, L-T., Li, Y. et al. (2023) MiPDCD6 effector suppresses host PAMP-triggered immunity to facilitate Meloidogyne incognita parasitism in tomato. Plant Pathology, 72, 195–206.

Kanehara, K., Cho, Y. & Yu, C.Y. (2022) A lipid viewpoint on the plant endoplasmic reticulum stress response. Journal of Experimental Botany, 73, 2835-2847.

Karimi, M., Inzé, D. & Ann, D. (2002) GATEWAYTM vectors for Agrobacterium-mediated plant transformation. Trends in Plant Science, 7, 193-195.

Karssen, G. & Moens, M. (1983) Root-knot nematodes. In: Perry, R.N and Moens, M. (Eds.) Plant Nematology. Wallingford, CABI, pp. 59-90.

Kaur, N. & Kaitheri Kandoth, P. (2021) Tomato bZIP60 mRNA undergoes splicing in endoplasmic reticulum stress and in response to environmental stresses. Plant Physiology and Biochemistry, 160, 397-403.

Köster, P., DeFalco, T.A. & Zipfel, C. (2022) Ca2+ signals in plant immunity. The EMBO Journal, 41, 1-18.

Kriechbaumer, V. & Brandizzi F. (2020). The plant endoplasmic reticulum: an organized chaos of tubules and sheets with multiple functions. Journal of Microscopy, 280, 122-133.

Kumar, A., Fitoussi, N., Sanadhya, P., Sichov, N., Bucki, P., Bornstein, M., et al. (2023) Two candidate Meloidogyne javanica effector genes, MjShKT and MjPUT3: a functional investigation of their roles in regulating nematode parasitism. Molecular Plant-Microbe Interactions, 36, 79-94.

Kamaruzzaman, M., Zhao, L.F., Zhang, J.A., Zhu, L.T., Li, Y. & Deng, X.D. et al. (2023) MiPDCD6 effector suppresses host PAMP-triggered immunity to facilitate Meloidogyne incognita parasitism in tomato. Plant Pathology, 72, 195-206.

Lacomme, C. & Santa Cruz, S. (1999) Bax-induced cell death in tobacco is similar to the hypersensitive response. Proceedings of the National Academy of Sciences, 96, 7956-7961.

Landry, D., Mila, I., Sabbagh, C.R.R., Zaffuto, M., Pouzet, C., Tremousaygue, D. et al. (2023) An NLR Integrated Domain toolkit to identify plant pathogen effector targets. The Plant Journal, 115, 1443-1457.

631 Lee, D.H., Lal, N.K., Lin, Z.J.D., Ma, S., Liu, J., Castro, B., et al. (2020) Regulation of reactive oxygen
632 species during plant immunity through phosphorylation and ubiquitination of RBOHD. Nature
633 Communications 11, 1838.
634 Li, J., Zhao-Hui, C., Batoux, M., Nekrasov, V., Roux, M., Chinchilla, D., et al. (2009) Specific ER
635 quality control components required for biogenesis of the plant innate immune receptor EFR.
636 Proceedings of the National Academy of Science USA, 106, 15973-15978.
637 Liu, J.X. & Howell, S.H. (2016) Managing the protein folding demands in the endoplasmic reticulum
638 of plants. The New phytologist, 211, 418-428.
639 Liu, J., Zhang, J., Wei, Y., Su, W., Li, W., Wang, B. et al. (2024) The nematode effector calreticulin
640 competes with the high mobility group protein OsHMGB1 for binding to the rice calmodulin-like
641 protein OsCML31 to enhance rice susceptibility to *Meloidogyne graminicola*. Plant, Cell &
642 Environment, 47, 1732–1746.
643 Lu, DP. & Christopher, D.A. (2008) Endoplasmic reticulum stress activates the expression of a sub-
644 group of protein disulfide isomerase genes and AtbZIP60 modulates the response in Arabidopsis
645 thaliana. Molecular Genetics and Genomics, 280, 199-210.
646 Makarova, S.S., Minina, E.A., Makarov, V.V., Semenyuk, P.I., Kopertekh, L., Schiemann, J. et al.
647 (2011) Orthologues of a plant-specific At-4/1 gene in the genus Nicotiana and the structural properties
648 of bacterially expressed 4/1 protein. Biochimie, 93, 1770-1778.
649 Mejias, J., Bazin, J., Truong, N.M., Chen, Y., Marteu, N., Bouteiller, N. et al. (2021) The root-knot
650 nematode effector MiEFF18 interacts with the plant core spliceosomal protein SmD1 required for giant
651 cell formation. New Phytologist, 229, 3408-3423.
652 Mejias, J., Chen, Y, Bazin, J., Truong, N.M., Mulet, K., Noureddine, Y., et al. (2022) Silencing the
653 conserved small nuclear ribonucleoprotein SmD1 target gene alters susceptibility to root-knot
654 nematodes in plants. Plant Physiology, 189, 1741-1756.
655 Michaud, M. & Jouhet, J. (2019) Lipid trafficking at membrane contact sites during plant development
656 and stress response. Frontiers in Plant Science, 10, 2.

Naalden, D., Haegeman, A., de Almeida-Engler, J., Birhane Eshetu, F., Bauters, L. & Gheysen, G. (2018) The Meloidogyne graminicola effector Mg16820 is secreted in the apoplast and cytoplasm to suppress plant host defense responses. Molecular Plant Patholohy, 19, 2416-2430.

Nekrasov, V., Li, J., Batoux, M., Roux, M., Chu, Z.H., Lacombe, S., et al. (2019) Control of the pattern-recognition receptor EFR by an ER protein complex in plant immunity. The EMBO Journal, 28, 3428-3438.

Nelson, B.K., Cai, X. & Nebenführ, A. (2007) A multicolored set of in vivo organelle markers for co-localization studies in Arabidopsis and other plants. Plant Journal, 51, 1126-1136.

Nguyen, H.P., Chakravarthy, S., Velásquez, A.C., McLane, H.L., Zeng, L., Nakayashiki, H. et al. (2010) Methods to study PAMP-triggered immunity using tomato and Nicotiana benthamiana. Molecular Plant-Microbe Interactions, 23, 991-999.

Nguyen, C.N., Perfus-Barbeoch, L., Quentin, M., Zhao, J., Magliano, M., Marteu, N. et al. (2018) A root-knot nematode small glycine and cysteine-rich secreted effector, MiSGCR1, is involved in plant parasitism. New Phytologist, 217, 687–699.

Niu, J., Liu, P., Liu, Q., Chen, C., Guo, Q., Yin, J. et al. (2016) Msp40 effector of root-knot nematode manipulates plant immunity to facilitate parasitism. Scientific Reports, 6,19443.

Pankratenko, A.V., Atabekova, A.K., Lazareva, E.A., Baksheeva, V.E., Zhironkina, O.A., Zernii, E.Y. et al. (2017) Plant-specific 4/1 polypeptide interacts with an endoplasmic reticulum protein related to human BAP31. Planta, 245: 193-205.

Park, C.J. & Seo, Y.S. (2015) Heat shock proteins: A review of the molecular chaperones for plant immunity. Plant Pathology Journal, 31, 323-333.

Quistgaard, E.M. (2021) BAP31: Physiological functions and roles in disease. Biochimie, 186, 105-129.

Rancurel, C., van Tran, T., Elie, C. & Hilliou, F. (2019) SATQPCR: Website for statistical analysis of real-time quantitative PCR data. Molecular and Cellular Probes, 46, 101418.

da Rocha M, Bournaud C, Dazenière J, Thorpe P, Bailly-Bechet M, Pellegrin C, et al. (2021) Genome expression dynamics reveal the parasitism regulatory landscape of the root-knot nematode Meloidogyne incognita and a promoter motif associated with effector genes. Genes 12, 771.

Rutter, W.B., Franco, J. & Gleason, C. (2022) Rooting out the mechanisms of root-knot nematode-plant interactions. Annual Review of Phytopathology, 60, 1-34.

Sacco, M.A., Koropacka, K., Grenier, E., Jaubert, M.J., Blanchard, A., Goverse, A. et al. (2009) The cyst nematode SPRYSEC protein RBP-1 elicits Gpa2- and RanGAP2-dependent plant cell death. PLoS Pathogens, 5, e1000564.

Sato, K., Kadota, Y. & Shirasu, K. (2019) Plant immune responses to parasitic nematodes. Frontiers in Plant Science, 10, 1165.

Siddique, S., Coomer, A., Baum, T. & Williamson, V.M. (2022) Recognition and response in plant-nematode interactions. Annual Review of Phytopathology, 60, 143-162.

Simoni, E.B., Oliveira, C.C., Fraga, O.T., Reis, P.A.B. & Fontes, E.P.B. (2022) Cell death signaling from endoplasmic reticulum stress: plant-specific and conserved features. Frontiers Plant Science, 13, 835738.

Song, H., Lin, B., Huang, Q., Sun, L., Chen, J., Hu, L. et al. (2021) The Meloidogyne graminicola effector MgMO289 targets a novel copper metallochaperone to suppress immunity in rice. Journal of Experimental Botany, 72, 5638-5655.

Strasser R. (2018) Protein quality control in the endoplasmic reticulum. Current Opinion in Cell Biology, 65, 96-102.

Thompson JD, Gibson TJ, Higgins DG. 2003. Multiple Sequence Alignment Using ClustalW and ClustalX. Current Protocols in Bioinformatics 1: 2–22.

Tian, T., Liu, Y., Yan, H., You, Q., Yi, X., Du, Z. et al. (2017) AgriGO v2.0: A GO analysis toolkit for the agricultural community, 2017 update. Nucleic Acids Research 45: W122–W129.

Truong, N.M., Chen, Y., Mejias, J., Soulé, S., Mulet, K., Jaouannet, M. et al. (2021) The Meloidogyne incognita nuclear effector MiEFF1 interacts with Arabidopsis cytosolic glyceraldehyde-3-phosphate dehydrogenases to promote parasitism. Front Plant Science, 12, 641480.

Vieira, P., Danchin, E.G., Neveu, C., Crozat, C., Jaubert, S., Hussey, R.S. et al. (2011) The plant apoplasm is an important recipient compartment for nematode secreted proteins. Journal of Experimental Botany, 62,1241-53.

711 Vieira, P. & Gleason, C. (2019) Plant-parasitic nematode effectors - insights into their diversity and new
712 tools for their identification. Current Opinion Plant Biology, 50, 37-43.
713 Wakana, Y., Takai, S., Nakajima, K., Tani, K., Yamamoto, A., Watson, P. et al. (2008) Bap31 is an
714 itinerant protein that moves between the peripheral endoplasmic reticulum (ER) and a juxtanuclear
715 compartment related to ER-associated Degradation. Molecular Biology of the Cell, 19, 1825-1836.
716 Wang, K., Remigi, P., Anisimova, M., Lonjon, F., Kars, I., Kajava, A. et al. (2016) Functional
717 assignment to positively selected sites in the core type III effector RipG7 from Ralstonia solanacearum.
718 Molecular Plant Pathology, 17, 553-564.
719 Yamaguchi, Y.L., Suzuki, R., Cabrera, J., Nakagami, S., Sagara, T., Ejima, C. et al. (2017) Root-knot
720 and cyst nematodes activate procambium-associated genes in arabidopsis roots. Frontiers in Plant
721 Science, 8, 1195.
722 Zhao, J., Huang, K., Liu, R., Lai, Y, Abad, P., Favery, B. et al. (2023) A root-knot nematode effector
723 Mi2G02 hijacks a host plant trihelix transcription factor for nematode parasitism. Plant
724 Communications, doi : 10.1016/j.xplc.2023.100723.
725 Zhao, J., Mejias, J., Quentin, M., Chen, Y., de Almeida-Engler, J., Mao, Z. et al. (2020) The root-knot
726 nematode effector MiPDI1 targets a stress-associated protein (SAP) to establish disease in Solanaceae
727 and Arabidopsis. New Phytologist, 228, 1417-1430.
728 Zhao, J., Sun, Q., Quentin, M., Ling, J., Abad, P., Zhang, X. et al. (2021) A Meloidogyne incognita C-
729 type lectin effector targets plant catalases to promote parasitism. New Phytologist 232, 2124-2137.
730 Zhuo, K., Chen, J., Lin, B., Wang, J., Sun, F., Hu, L. et al. (2017) A novel Meloidogyne enterolobii
731 effector MeTCTP promotes parasitism by suppressing programmed cell death in host plants.
732 Molecular Plant Pathology, 18, 45-54.
733

734 **SUPPORTING INFORMATION**

735 **Table S1.** Differentially expressed genes identified in the MiEFF12-expressing *Arabidopsis* line.

736 **Table S2.** Gene ontology (GO) analyses of the 1,103 genes upregulated in the MiEFF12a-expressing
737 line with a $\log_2 fd \geq 1$.

738 **Table S3.** List of 19 genes upregulated in the EFF12-expressing line and associated with GO term '
739 GO:0036293 response to decreased oxygen levels'.
740 **Table S4.** Gene ontology (GO) analyses of the 1,126 genes downregulated in the MiEFF12a-expressing
741 line with $log_2fd \leq -1$.
742 **Table S5.** List of 103 genes downregulated in the EFF12-expressing line and associated with GO term
743 ' GO:0006952 defense response'.
744 **Table S6.** Results of the yeast two-hybrid screen using MiEFF12a as a bait against the tomato root
745 cDNA library.
746 **Table S7.** Primers used in this study.
747 **Figure S1.** Amino acid sequences of EFF12 effector proteins identified in RKN species.
748 **Figure S2.** Nucleotide sequences of *EFF12*-encoding genes identified in RKN species.
749 **Figure S3.** Ectopic expression of MiEFF12a in Arabidopsis thaliana does not affect root development.
750 **Figure S4.** MiEFF12a interacts with SlPBL1, SlPBL2 and SlBZIP60 in yeast.
751 **Figure S5.** Nucleotide sequences of SlPBL1 and SlBZIP60
752 **Figure S6.** MiEFF12a and SlPBL1 colocalize in *N. benthamiana* epidermal leaf cells and both
753 MiEFF12a- and SlPBL1-GFP fusions were localized in large subcellular structures mostly juxtanuclear.
754 **Figure S7.** Nucleotide sequences of *N. benthamiana* BZIP60 and and design of the VIGS construct.
755 **Figure S8.** Plant BZIP60 is not required for *M. incognita* parasitism.
756 **Figure S9.** Nucleotide sequence of *N. benthamiana* PBL genes targeted by the VIGS approach.
757 **Figure S10.** MiEFF12a physically interacts in planta with NbPBL1a, NbPBL2a and NbPBL3a.
758 **Figure S11.** A chimeric sequence was introduced into the TRV2 RNA to silence the NbPBL genes
759 through VIGS.
760 **Figure S12.** The silencing of *PBL* genes by VIGS does not affect *N. benthamiana* root development.
761 **Figure S13.** MiEFF12a and SlPBL1a suppress flg22-mediated reactive oxygen species (ROS)
762 production in *Nicotiana benthamiana*.
763
764 **FIGURE LEGENDS**
765

Figure 1. Effector 12 (EFF12) is a conserved effector in root-knot nematodes. (a) Alignment of the MiEFF12 protein sequences. The green box indicates the position of the signal peptide for secretion. The conserved C-terminal region is enriched in positively (lysine-K) and negatively (asparagine-D and glutamic acid-E) charged residues. (b) Phylogenetic tree of *Meloidogyne* spp. EFF12 amino-acid sequences. The percentages displayed next to each branch represent the number of tree replicates in which the associated taxa were assembled together in 1,000 bootstraps. The lengths of the branches are not proportional to phylogenetic distance. (c) Pairwise sequence identity matrix for RKN *EFF12* nucleotide sequences.

Figure 2. The *Meloidogyne EFF12* genes are specifically expressed in the dorsal esophageal gland. *In situ* hybridization with specific antisense probes localized *EFF12* transcripts exclusively in the dorsal gland cell of pre-parasitic juveniles of *M. incognita* and *M. enterolobii*. Sense probes for *MiEFF12* and *MeEFF12* transcripts were used as a negative control and gave no signal. DG, dorsal gland. Bars = 20 µm.

Figure 3. The silencing of *MiEFF12* genes by host-induced gene silencing affects *M. incognita* parasitism. (a) Transcript quantification by RT-qPCR confirmed the effective silencing of *MiEFF12* genes in parasitic nematodes extracted from *N. benthamiana* roots infected with TRV2-MiEFF12 relative to controls (TRV2-empty and TRV2-GFP). Normalized relative transcript levels for three independent biological replicates are shown. (b) Infection test on *N. benthamiana* control plants (TRV2-empty and TRV2-GFP) and plants producing siRNA for the silencing of *MiEFF12* genes in *M. incognita* (TRV2-MiEFF12). Galls were counted six weeks after inoculation with 200 *M. incognita* second-stage juveniles per plant. Results from two independent experiments are shown (n=15 and n=17 plants for test N°1 and N°2, respectively). The cross represents average value. Box indicates interquartile range (25^{th} to the

75th percentile). The central line within the box represents mean value. Whiskers indicate the minimum and maximum values for the normal values present in the dataset. Statistical significance was assessed in Student's *t* tests. Significant differences were observed between controls and TRV-MiEFF12 plants (* $p < 0.05$).

Figure 4. MiEFF12 suppress host defense responses. (a-b) Gene ontology (GO) enrichment analysis of DEGs in the *Arabidopsis* MiEFF12a-expressing line with AgriGO v2.0. (a) GO enrichment analysis for the 1,103 genes upregulated in the MiEFF12a-expressing line with $\log_2 fd \geq 1$, indicating an enrichment in genes related to the response to decreased oxygen levels. (b) GO enrichment analysis on the 1,126 genes downregulated in the MiEFF12a-expressing line with $\log_2 fd \leq -1$, indicating an enrichment in genes related to the defense response. (c) MiEFF12 suppresses flg22-mediated reactive oxygen species (ROS) production in *Nicotiana benthamiana*. *Agrobacterium tumefaciens* strain GV3101 carrying MiEFF12a was used to infiltrate the leaves of *N. benthamiana* plants. Infiltrated leaf discs were collected 48 h post-agroinfiltration and assayed for ROS production in response to treatment with the flg22 elicitor. ROS production was monitored for 40 min, and the values shown are the mean relative luminescence units ± SD for 28 leaf discs. (d) BAX-triggered cell death was not suppressed by MiEFF12a. Photographs for assessment of the cell-death phenotype were taken five days after the last infiltration. (e) Gpa2/RBP-1-triggered cell death was suppressed by MiEFF12a. Photographs showing the suppression of cell death were taken five days after the last infiltration. Each cell death suppression bioassay was performed at least three times; results from a representative experiment are shown.

Figure 5. MiEFF12a was localized to the endoplasmic reticulum (ER) of epidermal *Nicotiana benthamiana* leaf cells. (a) Single-plane confocal images of *N. benthamiana* leaf cells infiltrated

with *Agrobacterium tumefaciens* and producing MiEFF12a without its signal peptide, fused to the C-terminal end of the green fluorescent protein (GFP) reporter (GFP-MiEFF12a; green signal; left pictures). Overlays of differential interference contrast and fluorescence images are shown (right pictures). **(**b) Single-plane confocal images of *N. benthamiana* leaf cells infiltrated with *A. tumefaciens* and producing MiEFF12a without the signal peptide, fused to the N-terminal end of the green fluorescent protein (GFP) reporter (MiEFF12a-GFP; green signal; left pictures). Overlays of differential interference contrast and fluorescence images are shown (right pictures). (c) The monomeric red fluorescent protein (mRFP) signal (RFP-ER; red signal) of an ER marker was used to analyze colocalization of the GFP-MiEFF12a fusion (green signal) and the ER. (d) The mRFP signal (red signal) of the ER marker was used to analyze its co-localization with the MiEFF12a-GFP fusion (green signal). Both fusions between the GFP and MiEFF12a colocalized with the ER marker in *N. benthamiana* leaf cells. Asterisk; nucleus. Scale bars: 20 μm.

Figure 6. MiEFF12a physically interacts *in planta* with SlPBL1 and SlBZIP60. SlPBL1 and SlBZIP60 co-localized localized with MiEFF12a in the endoplasmic reticulum (ER) of epidermal *Nicotiana benthamiana* leaf cells. (a) Single-plane confocal images of *N. benthamiana* leaf cells infiltrated with *Agrobacterium tumefaciens* and producing SlPBL1, fused to the C-terminal end of the green fluorescent protein (GFP) reporter (GFP-SlPBL1; green signal) and MiEFF12a fused to the c-terminal end of the red fluorescent protein (RFP) reporter (RFP-MiEFF12a; red signal). **(**b) Single-plane confocal images of *N. benthamiana* leaf cells infiltrated with *Agrobacterium tumefaciens* and producing SlBZIP60, fused to the C-terminal end of the green fluorescent protein (GFP) reporter (GFP-SlBZIP60; green signal) and the RFP-MiEFF12a recombinant protein (RFP-MiEFF12a: red signal). Overlays of fluorescence images are shown (merge). Scale bars: 20 μm. (c) Schematic representation of the full-length (tot, total)

and truncated (sol, soluble) SlPBL1 and SlBZIP60 proteins used for interactomic assays. (d) Co-immunoprecipitation experiments confirmed that MiEFF12a interacted with the full-length SlPBL1 and BZIP60. SlPBLtot-GFP, SlPBLsol-GFP or SlBZIP60 were transiently co-expressed with MiEFF12a–HA or MiCRT in tobacco leaves. The Co-IP experiment was performed with anti-HA affinity gel, and the protein isolated was analyzed by immunoblotting with anti-GFP antibodies to detect SlPBLtot and SlPBLsol, and with anti-HA antibodies to detect MiEFF12a and MiCRT. Three independent experiments were performed, with similar results.

Figure 7. The silencing of *PBL* genes in *N. benthamiana* affects susceptibility to *M. incognita*. (a) Timeline used for virus-induced gene silencing (VIGS) experiments. (b) RT-qPCR showing the efficient silencing of the *NbPBL1a/b*, *NbPBL2a/b* and *NbPBL3a/b* gene pairs in *N. benthamiana* control plants (TRV-GFP) and plants in which *NbPBLs* were silenced (TRV2-PBLs). The data shown are normalized relative transcript levels for three independent biological replicates obtained with SatqPCR software. The *NbEF1a* and *NbGADPH* housekeeping genes were used for data normalization. Error bars indicate the SEM. (c) Infection test on *N. benthamiana* TRV-GFP or TRV2-PBLs plants. Galls were counted six weeks after inoculation with 200 *M. incognita* second-stage juveniles (J2s) per plant. Results from three independent experiments are shown (n=19, n=15 and n= 21 plants for test N°1, N°2 and N°3, respectively). The cross represents average value. Box indicates interquartile range (25th to the 75th percentile). The central line within the box represents mean value. Whiskers indicate the minimum and maximum values for the normal values present in the dataset. Statistical significance was determined in Student's *t* test and significant differences were observed between TRV-GFP control and TRV-PBL plants (* $p < 0.01$).

866

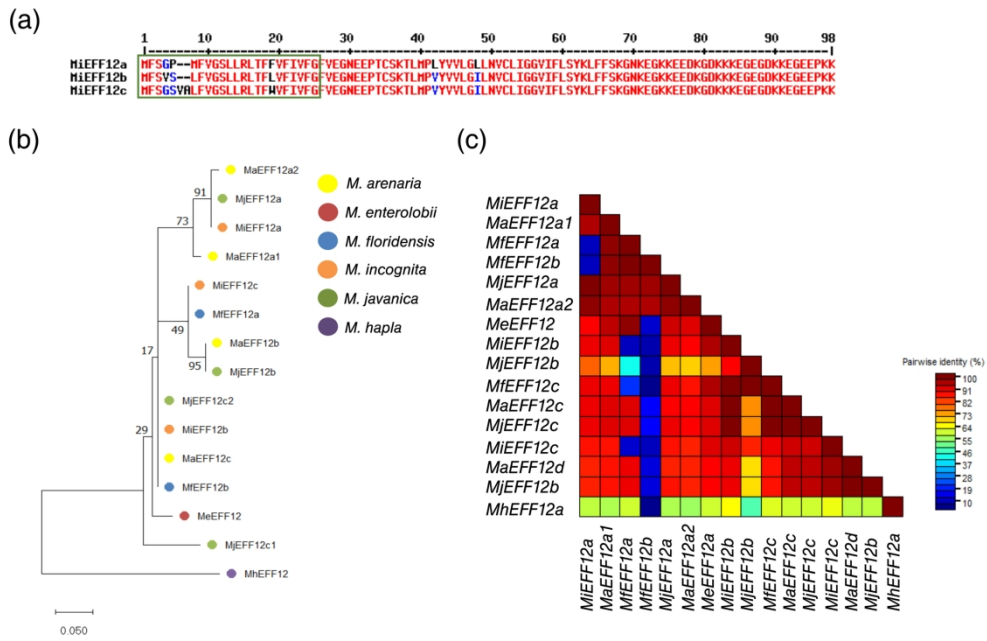

Figure 1. Effector 12 (EFF12) is a conserved effector in root-knot nematodes. (a) Alignment of the MiEFF12 protein sequences. The green box indicates the position of the signal peptide for secretion. The conserved C-terminal region is enriched in positively (lysine-K) and negatively (asparagine-D and glutamic acid-E) charged residues. (b) Phylogenetic tree of Meloidogyne spp. EFF12 amino-acid sequences. The percentages displayed next to each branch represent the number of tree replicates in which the associated taxa were assembled together in 1,000 bootstraps. The lengths of the branches are not proportional to phylogenetic distance. (c) Pairwise sequence identity matrix for RKN EFF12 nucleotide sequences.

183x123mm (300 x 300 DPI)

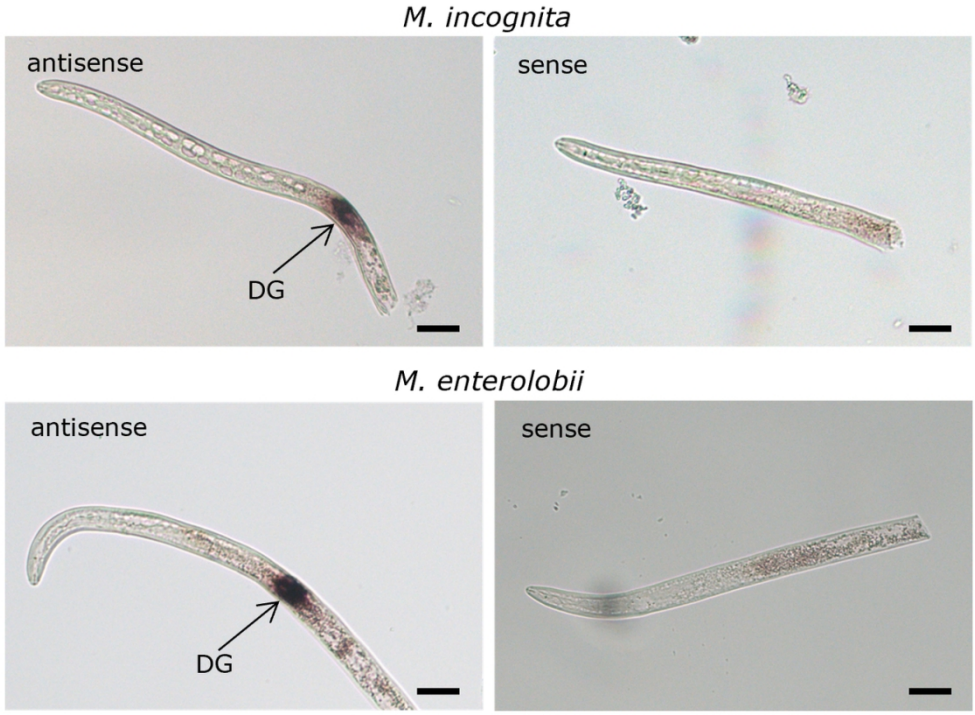

Figure 2. The Meloidogyne EFF12 genes are specifically expressed in the dorsal esophageal gland. In situ hybridization with specific antisense probes localized EFF12 transcripts exclusively in the dorsal gland cell of pre-parasitic juveniles of M. incognita and M. enterolobii. Sense probes for MiEFF12 and MeEFF12 transcripts were used as a negative control and gave no signal. DG, dorsal gland. Bars = 20 µm.

115x87mm (300 x 300 DPI)

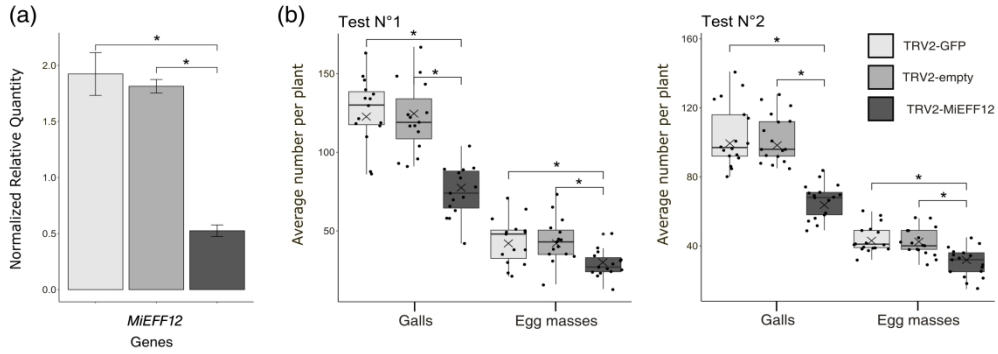

Figure 3. The silencing of MiEFF12 genes by host-induced gene silencing affects M. incognita parasitism. (a) Transcript quantification by RT-qPCR confirmed the effective silencing of MiEFF12 genes in parasitic nematodes extracted from N. benthamiana roots infected with TRV2-MiEFF12 relative to controls (TRV2-empty and TRV2-GFP). Normalized relative transcript levels for three independent biological replicates are shown. (b) Infection test on N. benthamiana control plants (TRV2-empty and TRV2-GFP) and plants producing siRNA for the silencing of MiEFF12 genes in M. incognita (TRV2-MiEFF12). Galls were counted six weeks after inoculation with 200 M. incognita second-stage juveniles per plant. Results from two independent experiments are shown (n=15 and n=17 plants for test N°1 and N°2, respectively). The cross represents average value. Box indicates interquartile range (25th to the 75th percentile). The central line within the box represents mean value. Whiskers indicate the minimum and maximum values for the normal values present in the dataset. Statistical significance was assessed in Student's t tests. Significant differences were observed between controls and TRV-MiEFF12 plants (* $p < 0.05$).

335x118mm (300 x 300 DPI)

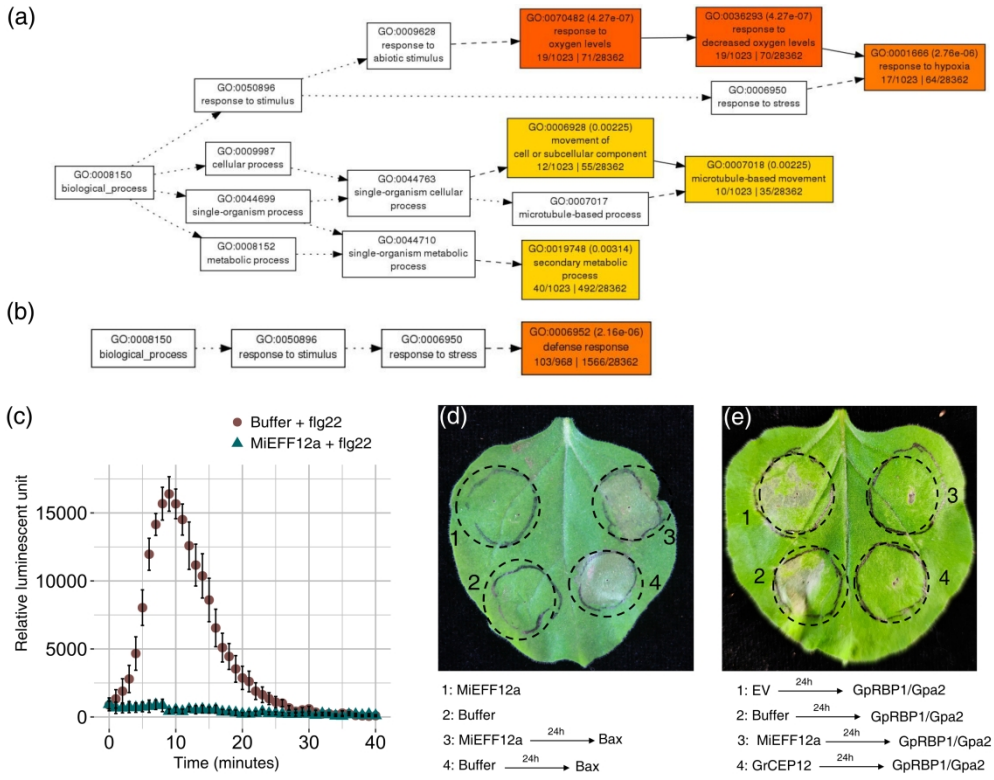

Figure 4. MiEFF12 suppress host defense responses. (a-b) Gene ontology (GO) enrichment analysis of DEGs in the Arabidopsis MiEFF12a-expressing line with AgriGO v2.0. (a) GO enrichment analysis for the 1,103 genes upregulated in the MiEFF12a-expressing line with log2fd≥1, indicating an enrichment in genes related to the response to decreased oxygen levels. (b) GO enrichment analysis on the 1,126 genes downregulated in the MiEFF12a-expressing line with log2fd≤-1, indicating an enrichment in genes related to the defense response. (c) MiEFF12 suppresses flg22-mediated reactive oxygen species (ROS) production in Nicotiana benthamiana. Agrobacterium tumefaciens strain GV3101 carrying MiEFF12a was used to infiltrate the leaves of N. benthamiana plants. Infiltrated leaf discs were collected 48 h post-agroinfiltration and assayed for ROS production in response to treatment with the flg22 elicitor. ROS production was monitored for 40 min, and the values shown are the mean relative luminescence units ± SD for 28 leaf discs. (d) BAX-triggered cell death was not suppressed by MiEFF12a. Photographs for assessment of the cell-death phenotype were taken five days after the last infiltration. (e) Gpa2/RBP-1-triggered cell death was suppressed by MiEFF12a. Photographs showing the suppression of cell death were taken five days after the last infiltration. Each cell death suppression bioassay was performed at least three times; results from a representative experiment are shown.

354x277mm (300 x 300 DPI)

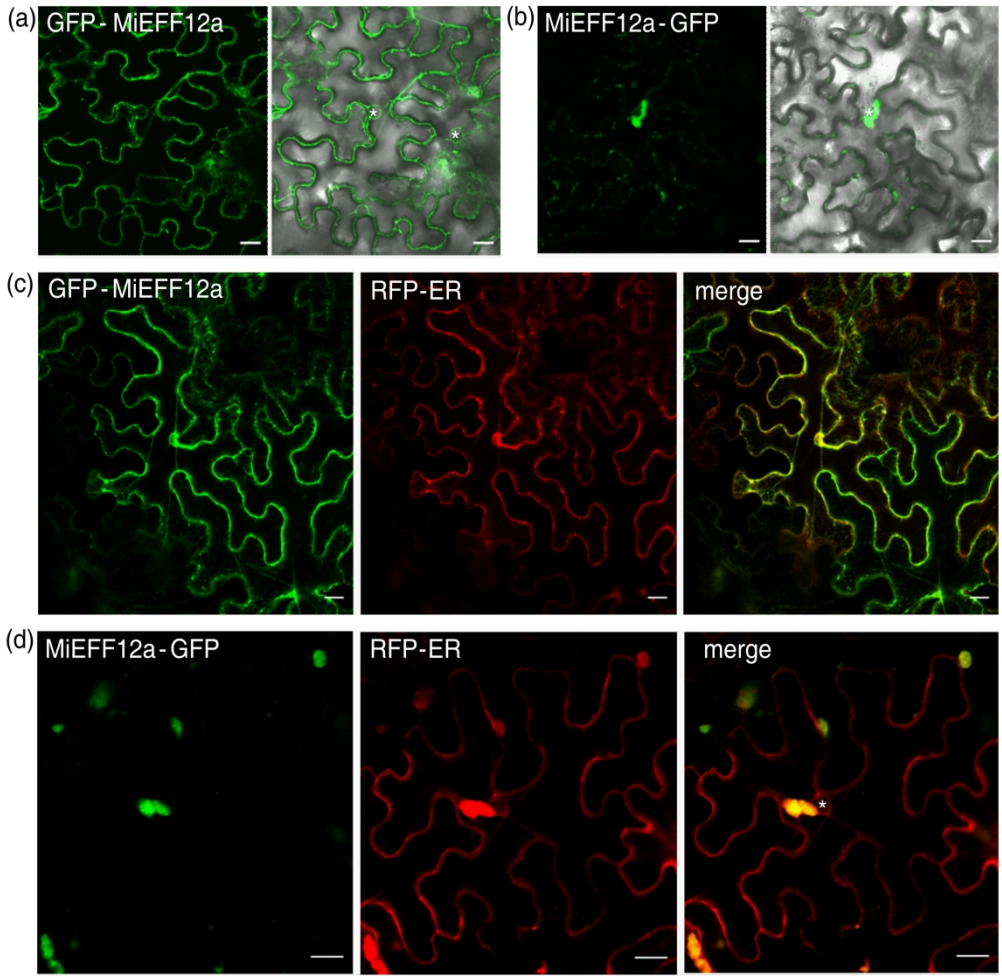

Figure 5. MiEFF12a was localized to the endoplasmic reticulum (ER) of epidermal Nicotiana benthamiana leaf cells. (a) Single-plane confocal images of N. benthamiana leaf cells infiltrated with Agrobacterium tumefaciens and producing MiEFF12a without its signal peptide, fused to the C-terminal end of the green fluorescent protein (GFP) reporter (GFP-MiEFF12a; green signal; left pictures). Overlays of differential interference contrast and fluorescence images are shown (right pictures). (b) Single-plane confocal images of N. benthamiana leaf cells infiltrated with A. tumefaciens and producing MiEFF12a without the signal peptide, fused to the N-terminal end of the green fluorescent protein (GFP) reporter (MiEFF12a-GFP; green signal; left pictures). Overlays of differential interference contrast and fluorescence images are shown (right pictures). (c) The monomeric red fluorescent protein (mRFP) signal (RFP-ER; red signal) of an ER marker was used to analyze colocalization of the GFP-MiEFF12a fusion (green signal) and the ER. (d) The mRFP signal (red signal) of the ER marker was used to analyze its co-localization with the MiEFF12a-GFP fusion (green signal). Both fusions between the GFP and MiEFF12a colocalized with the ER marker in N. benthamiana leaf cells. Asterisk; nucleus. Scale bars: 20 μm.

225x226mm (300 x 300 DPI)

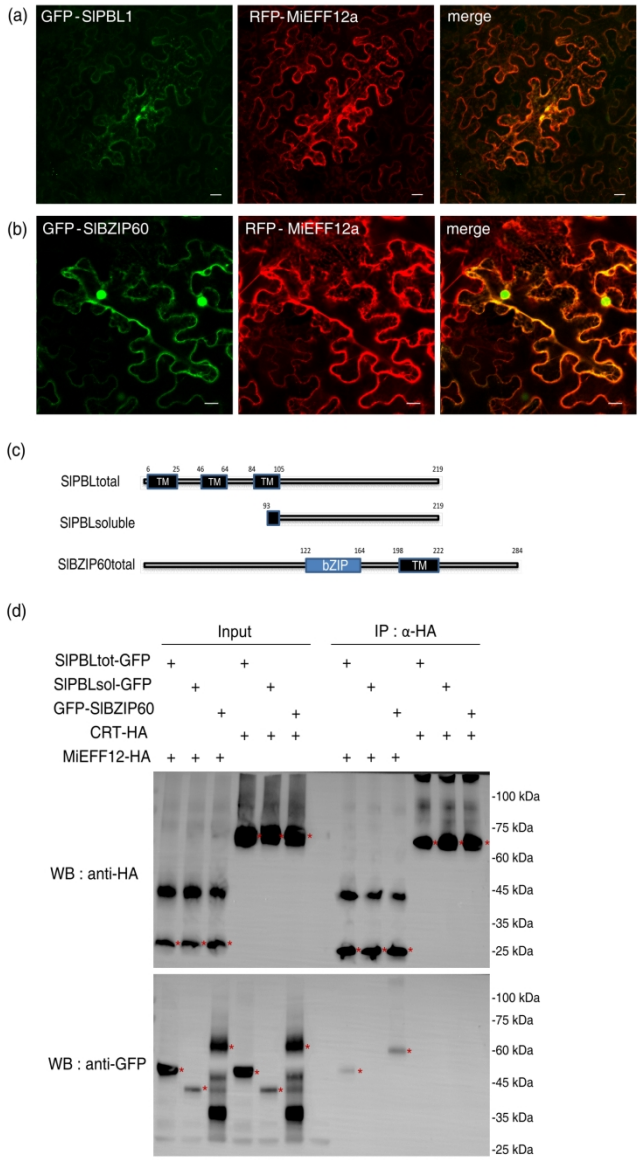

Figure 6. MiEFF12a physically interacts in planta with SlPBL1 and SlBZIP60. SlPBL1 and SlBZIP60 co-localized localized with MiEFF12a in the endoplasmic reticulum (ER) of epidermal Nicotiana benthamiana leaf cells. (a) Single-plane confocal images of N. benthamiana leaf cells infiltrated with Agrobacterium tumefaciens and producing SlPBL1, fused to the C-terminal end of the green fluorescent protein (GFP) reporter (GFP-SlPBL1; green signal) and MiEFF12a fused to the c-terminal end of the red fluorescent protein (RFP) reporter (RFP-MiEFF12a; red signal). (b) Single-plane confocal images of N. benthamiana leaf cells infiltrated with Agrobacterium tumefaciens and producing SlBZIP60, fused to the C-terminal end of the green fluorescent protein (GFP) reporter (GFP-SlBZIP60; green signal) and the RFP-MiEFF12a recombinant protein (RFP-MiEFF12a: red signal). Overlays of fluorescence images are shown (merge). Scale bars: 20 μm. (c) Schematic representation of the full-length (tot, total) and truncated (sol, soluble) SlPBL1 and SlBZIP60 proteins used for interactomic assays. (d) Co-immunoprecipitation experiments confirmed that MiEFF12a interacted with the full-length SlPBL1 and BZIP60. SlPBLtot-GFP, SlPBLsol-GFP or SlBZIP60 were transiently co-expressed with MiEFF12a–HA or MiCRT in tobacco leaves. The Co-IP experiment was performed with anti-HA affinity gel, and the protein isolated was analyzed by immunoblotting with anti-GFP antibodies to detect

SlPBLtot and SlPBLsol, and with anti-HA antibodies to detect MiEFF12a and MiCRT. Three independent experiments were performed, with similar results.

138x243mm (300 x 300 DPI)

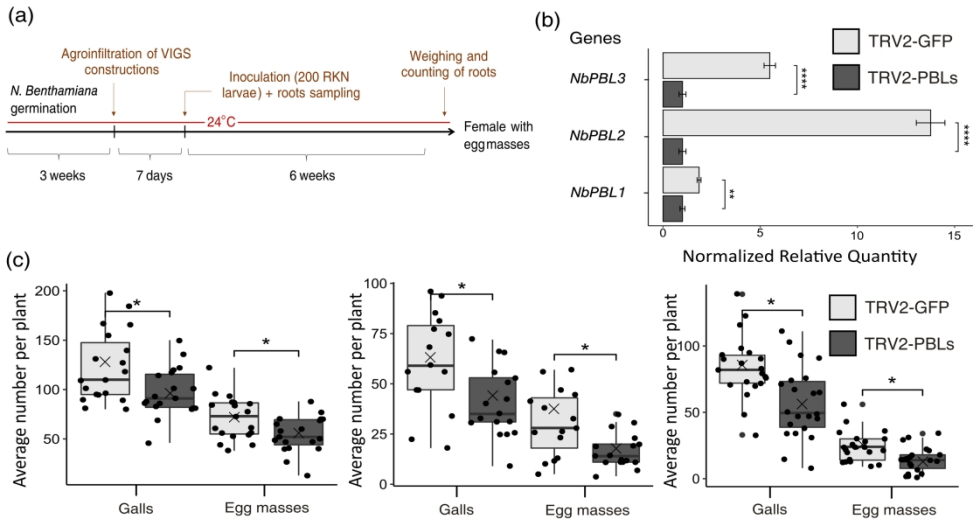

Figure 7. The silencing of PBL genes in N. benthamiana affects susceptibility to M. incognita. (a) Timeline used for virus-induced gene silencing (VIGS) experiments. (b) RT-qPCR showing the efficient silencing of the NbPBL1a/b, NbPBL2a/b and NbPBL3a/b gene pairs in N. benthamiana control plants (TRV-GFP) and plants in which NbPBLs were silenced (TRV2-PBLs). The data shown are normalized relative transcript levels for three independent biological replicates obtained with SatqPCR software. The NbEF1a and NbGADPH housekeeping genes were used for data normalization. Error bars indicate the SEM. (c) Infection test on N. benthamiana TRV-GFP or TRV2-PBLs plants. Galls were counted six weeks after inoculation with 200 M. incognita second-stage juveniles (J2s) per plant. Results from three independent experiments are shown (n=19, n=15 and n= 21 plants for test N°1, N°2 and N°3, respectively). The cross represents average value. Box indicates interquartile range (25th to the 75th percentile). The central line within the box represents mean value. Whiskers indicate the minimum and maximum values for the normal values present in the dataset. Statistical significance was determined in Student's t test and significant differences were observed between TRV-GFP control and TRV-PBL plants (* $p < 0.01$).

242x133mm (300 x 300 DPI)